HHS Public Access

Author manuscript

Nano Lett. Author manuscript; available in PMC 2018 July 20.

Published in final edited form as:

Nano Lett. 2018 March 14; 18(3): 2148–2157. doi:10.1021/acs.nanolett.8b00432.

A direct comparison of i*n vitro* and *in vivo* nucleic acid delivery mediated by hundreds of nanoparticles reveals a weak correlation

Kalina Paunovska[1,*], **Cory D. Sago**[1,*], **Christopher M. Monaco**[1,2], **William H. Hudson**[3], **Marielena Gamboa Castro**[1], **Tobi G. Rudoltz**[1], **Sujay Kalathoor**[1], **Daryll A. Vanover**[1], **Philip J. Santangelo**[1], **Rafi Ahmed**[3], **Anton V. Bryksin**[4], and **James E. Dahlman**[1]

[1]Wallace H. Coulter Department of Biomedical Engineering, Georgia Institute of Technology and Emory University School of Medicine, Atlanta, Georgia, 30332, USA

[2]School of Biological Sciences, Georgia Institute of Technology, Atlanta, Georgia, 30332, USA

[3]Emory Vaccine Center and Department of Microbiology and Immunology, Emory University School of Medicine, Atlanta, Georgia, 30317, USA

[4]Parker H. Petit Institute for Bioengineering and Bioscience, Georgia Institute of Technology, Atlanta, Georgia, 30332, USA

Abstract

Endothelial cells and macrophages play active roles in disease, and as a result, are important targets for nucleic acid therapies. While thousands of chemically distinct lipid nanoparticles (LNPs) can be synthesized to deliver nucleic acids, studying more than a few LNPs *in vivo* is challenging. As a result, it is difficult to understand how nanoparticles target these cells *in vivo*. Using high throughput LNP barcoding, we quantified how well LNPs delivered DNA barcodes to endothelial cells and macrophages *in vitro*, as well as endothelial cells and macrophages isolated from the lung, heart, and bone marrow *in vivo*. We focused on two fundamental questions in drug delivery. First, does *in vitro* LNP delivery predict *in vivo* LNP delivery? By comparing how 281 LNPs delivered barcodes to endothelial cells and macrophages *in vitro* and *in vivo*, we found *in vitro* delivery did not predict *in vivo* delivery. Second, does LNP delivery change within the microenvironment of a tissue? We quantified how 85 LNPs delivered barcodes to eight splenic cell populations, and found that cell types derived from myeloid progenitors tended to be targeted by similar LNPs, relative to cell types derived from lymphoid progenitors. These data demonstrate that barcoded LNPs can elucidate fundamental questions about *in vivo* nanoparticle delivery.

To whom correspondence should be addressed: james.dahlman@bme.gatech.edu.

*K.P. and C.D.S. contributed equally to this work.

Roles. K.P., C.D.S., and J.E.D. designed experiments. All authors performed the experiments and/or analyzed the data. K.P., C.D.S., and J.E.D. wrote the paper with input from all authors.

Supporting Information Available: Barcode sequences used, NGS primers, normalization procedure, *in vitro* barcode imaging; library 1 design, *in vitro* dose response; FACs gating strategies for endothelial cells and macrophages, library 2 and 3 design, LNP diameter distributions, *in vitro* vs. *in vivo* and primary cell dataset complementing figure 2; macrophage dataset complementing figure 4A–B, *in vivo* endothelial cells and macrophages plotted according to *in vitro* rank, LNP structures and supporting information for ranked particles in endothelial cells and macrophages, significant and non-significant relationships between LNP structure and cell targeting; LNP library used for spleen biodistribution, FACs gating strategy for spleen; mouse weights for all experiments relative to control (PBS).

Keywords

DNA barcoded nanoparticles; nanotechnology; drug delivery; siRNA; gene editing

Introduction

The transport of foreign nucleic acids is carefully regulated, making systemic drug delivery inefficient[1–3]. To deliver nucleic acids, thousands of chemically distinct lipid nanoparticles (LNPs) have been designed[4–9]. LNP chemical diversity is imparted 2 ways. First, thousands of distinct biomaterials have been synthesized[4–9]. Second, each biomaterial can be formulated into hundreds of LNPs by adding poly(ethylene glycol) (PEG), cholesterol, 1,2-dioleoyl-*sn*-glycero-3-phosphoethanolamine (DOPE), and other constituents at different mole ratios. LNPs are screened *in vitro* before a small number of finalists is tested *in vivo*[4–9]; in a typical example, we measured how well 2,000 LNPs delivered siRNA to HeLa cells in static cell culture before analyzing 5 LNPs *in vivo*[5]. Similar studies have been performed with LNPs composed of small amine-, sugar-, or peptide-based materials[4, 6–9].

To successfully deliver nucleic acids after systemic administration, nanoparticles must overcome complex obstacles that are difficult to model *in vitro*. A significant fraction of the drug can be lost at each point, and as a result, every step is important to model. For example, cationic nanoparticles can be disassembled by the renal anionic basement membrane[10], and nanoparticles can be blocked from accessing brain parenchyma, due to the capillary tight junctions and glial cells that make up the blood brain barrier[11–15]. By contrast, nanoparticles can access tissues like the liver via porous ECs and discontinuous basement membranes in the hepatic sinusoids[11–15]. In addition to these barriers, blood flow rates affect nanoparticle targeting by affecting the likelihood a particle leaves the bloodstream[16].

Despite these differences, nanoparticles are often screened *in vitro.* Large scale *in vitro* nanoparticle screens typically utilize cells that are easy to expand (e.g. HeLa)[4–9]. These cells have genotypes and phenotypes that differ from cells *in vivo.* Cells can also undergo significant changes in gene expression when cultured[17]. Many of these changes may be driven by exposure to a combination of foreign serum (e.g. FBS) and static fluid flow, which most cell types are not exposed to *in vivo*. Given that *in vitro* and *in vivo* delivery require the nanoparticle to overcome different physiological obstacles, and that endocytosis is likely to be affected by gene expression changes that occur when cells are removed from their natural microenvironment, we hypothesized that *in vivo* LNP delivery would not be predicted *in vitro* using common cell culture conditions.

The field can currently synthesize nanomaterials at a rate several orders of magnitude higher than the rate at which we can test nanomaterials for drug delivery *in vivo.* Recently, we reported a nanoparticle DNA barcoding system[18] to increase the number of LNPs we could study at once *in vivo*. We used a microfluidic device to barcode LNPs (Fig. 1A)[19]; each LNP was formulated to carry a unique DNA barcode. We pooled stable LNPs, administered them to animals, and deep sequenced the barcodes to quantify the delivery of up to 30 LNPs simultaneously[18]. This original paper focused exclusively on control experiments designed to characterize the system. Specifically, we demonstrated that barcoded LNPs can be made

so they do not mix in solution, that DNA sequencing readouts were linear with respect to the amount of injected DNA, that DNA barcode delivery recapitulates the behavior of previously characterized LNPs, that delivery does not change with DNA sequence, and that delivery of DNA barcodes to hepatocytes *in vivo* modeled siRNA delivery to hepatocytes *in vivo*[18].

We now report that the same LNP barcoding system, herein named JOint Rapid DNA Analysis of Nanoparticles (JORDAN), can elucidate fundamental questions about nanoparticle delivery. We quantified how well 281 LNPs delivered DNA barcodes to endothelial cells and macrophages, both *in vitro* and *in vivo*. We focused on endothelial cells and macrophages for three reasons. First, both cell types are implicated in many diseases[20, 21]. Second, since they are ubiquitous, we could measure delivery to the same cell type in multiple tissues. Third, endothelial cells are more 'accessible' upon intravenous injection than tissue macrophages. We reasoned, incorrectly, that delivery to more accessible cells would be more predictable *in vitro*. Our data strongly suggest that *in vitro* LNP delivery to endothelial cells and macrophages using static cell culture does not predict *in vivo* LNP delivery to the same cell types.

We then used the JORDAN system to investigate how different LNPs distribute within the spleen, an important clearance organ. By measuring how 85 LNPs delivered barcodes to 8 different splenic cell types, we found that cells derived from myeloid progenitors tended to be targeted to by similar LNPs; cells derived from lymphoid progenitors tended to be targeted by different LNPs. We then identified LNP1, which delivered barcodes to all 8 cell types we studied in the spleen. We confirmed the splenic targeting of LNP1 using fluorescently labeled DNA. The approach we have described can be extended to study (i) how well any *in vitro* system (e.g. tissue-on-a-chip) predicts delivery *in vivo,* and (ii) how different cells are targeted within a tissue.

Results

We rationally designed DNA barcodes in order to study the delivery of many LNPs at once (Fig. 1A–C). Each DNA barcode contained phosphorothioate linkages in order to reduce exonuclease activity, and universal primer sites for unbiased PCR amplification (Fig. 1C)[18]. The 8 nucleotide 'barcode' region was located in the middle of the 56 nucleotide DNA sequence. Of the 4^8 possible DNA barcode combinations, we designed 240 to work with Illumina sequencing machines (Fig. S1A). We amplified barcodes using universal primers and labeled individual samples with Illumina dual-indexed adapters that enabled sample multiplexing (Fig. S1B). For each experiment, we calculated the 'normalized delivery', using the administered LNP solution as a DNA input (Fig. 1D, Fig. S1C). We also added new LNP quality controls to reduce the likelihood LNPs mixed together. Specifically, we analyzed the size of each individual LNP using dynamic light scattering (DLS). Based on our experience studying LNPs[5, 18, 22–25], we only pooled stable LNPs with good autocorrelation curves and diameters between 20 and 300 nm (Fig. S1D). We then tested whether barcoded LNPs entered cells. We formulated Alexa647-tagged DNA barcodes in a previously characterized[5, 18, 22–27] LNP named 7C1. Barcodes entered immortalized mouse aortic endothelial cells (iMAECs) within 15 minutes, and were observed inside the cell at 1.5 and 72 hours after administration (Fig. 1E, Fig. S1E, F).

We then formulated a library of 144 LNPs, library 1, systematically varying PEG structure. We synthesized 2 biomaterials called 'lipomers', which are lipid-amines conjugates created by reacting epoxide, acrylate, or methacrylate-terminated lipids with oligoamines[5, 7, 18, 28, 29]. Both lipomers were formulated into 72 LNPs, using 9 different PEGs and 8 different PEG mole percentages, for a total of 144 LNPs (Fig. 2A, Fig. S2A). 112 out of 144 formulations formed stable LNPs and were pooled (Fig. 2B). We administered the 112 stable LNPs, as well as a naked DNA barcode - which served as a negative control - to cells at a total DNA dose of 4, 20, and 100 ng/well, in a 24 well plate. Concurrently, we administered the LNPs to mice via a tail vein injection at a total dose of 0.5 mg/kg DNA. We isolated DNA from cells or tissues 72 hours later, a time point we chose to minimize the influence of dynamic endocytic processes[5, 30–33]. The 4 ng total DNA dose equaled an average DNA dose of 0.035 ng/well/LNP, demonstrating the sensitivity of the DNA barcoding system. We administered the LNPs to immortalized mouse aortic endothelial cells (iMAECs), and mouse macrophages (RAWs). We chose iMAECs since they are isolated directly from the murine heart, and have been shown to recapitulate endothelial cell signaling and function[34]. We chose RAWs since they are a commonly used macrophage cell line.

We examined positive and negative controls to evaluate whether this dataset was robust. The naked barcode (negative control) performed poorly compared to LNP-delivered DNA in all 18 samples (Fig. 2C, D). LNP delivery in iMAECs and RAWs treated with 20 ng total DNA predicted LNP delivery in iMAECs and RAWs treated with 4 or 100 ng DNA with high precision ($R^2 > 0.9$) (Fig. 2E, Fig. S2B–D). Put another way, in this positive control experiment, delivery to iMAECs *in vitro* at 1 dose predicted delivery to iMAECs at 2 other doses.

We then investigated whether *in vitro* LNP delivery predicted *in vivo* LNP delivery (Fig. 3A). We compared normalized delivery in iMAECs and RAWs to endothelial cells (ECs) and macrophages isolated from mice injected with LNPs. We isolated endothelial cells and macrophages from mice using a fluorescence activated cell sorting (FACS) protocol we previously established[5, 18, 22, 26] (Fig. S3A–C). *In vitro* iMAEC delivery did not predict *in vivo* delivery to heart, lung, or bone marrow endothelial cells (Fig. S3J–L). Similarly, delivery to RAWs *in vitro* did not predict delivery to heart, lung, or bone marrow macrophages (Fig. S3S–U). To validate these results, we synthesized two additional LNP libraries. Library two consisted of 120 LNPs, of which 105 were found to be stable by DLS, and included (Fig. S3D,E). In this library, we systematically varied the lipid tail and amine reacted to make the lipomer component of each LNP. Library three consisted of 156 LNPs, of which 64 were found to be stable by DLS, and included (Fig. S3F,G). In this library, we systematically varied the PEG tail length and molecular weight (MW), using three different tail lengths (C14, C16, C18) and 2 different MWs (350, 2000 Da). Results from libraries two and three recapitulated results from library one; *in vitro* delivery to endothelial cells and macrophages did not predict *in vivo* delivery to the same cell types. In total, we performed three experiments, formulating 420 LNPs, of which 281 were stable and included (Fig. S3H–I). Results from each individual experiment are plotted in Supplementary Fig. 3J–AA. Combined results from all 3 experiments are plotted in Fig. 3B–G.

We considered the possibility that our results were due to a poor choice of cell line or time-point. To exclude this possibility, we investigated to what extent the (i) cell line and (ii) experimental time point altered the predictivity of *in vitro* delivery. We performed these experiments using library two. We administered library two to iMAECs, RAWs, and mice, and measured delivery 4, 48, and 72 hours after LNP administration (Fig. S3M–O, V–X, BB–LL). At all three time points, we also measured LNP delivery to three primary human endothelial cell lines: human aortic endothelial cells (HAECs), human aortic vein endothelial cells (HAVECs), and human umbilical vein endothelial cells (HUVECs). In all cases, we observed no strong relationship between *in vitro* and *in vivo* delivery (Fig. S3MM–UU).

We then analyzed our data set, with the goal of quantifying the 'efficiency' of traditional *in vitro* screening. Put another way, if a LNP library is screened *in vitro* and a small number of LNPs is selected for *in vivo* analysis, how likely is it that the best *in vivo* candidate is selected? We first calculated the percentage of an *in vitro* library required to select the top 5, 10, 15, or 20% of *in vivo* LNPs. To ensure the top 5% of *in vivo* LNPs were selected, more than 50% of the *in vitro* library would need to be selected (Fig. 4A, Fig. S4A). We then analyzed how well the best *in vivo* LNPs performed *in vitro.* We ranked LNPs based on their *in vitro* performance. We then colored the LNPs that performed in the top 10% *in vivo* and listed their respective LNP compositions and sizes (Fig. S4D–G). Some LNPs that performed well *in vivo* also performed well *in vitro*. However, in many cases, LNPs that performed well *in vivo* did not rank highly *in vitro*; these LNPs would likely be discarded after an *in vitro* screen. Third, we evaluated how the top *in vitro* LNPs performed *in vivo.* Top ranked *in vitro* LNPs did not consistently perform well *in vivo* (Fig. 4B, Fig. S4B). More specifically, we plotted the *in vivo* rank (Y axis) for each of the top 5 *in vitro* LNPs and found that the top 5 *in vitro* LNPs often performed poorly *in vivo.* This result was consistent for 3 *in vivo* endothelial beds (Fig. 4B), as well *in vivo* macrophages from three tissues (Fig. S4B). Based on this result, we asked a fourth question: if we selected the top 3, 5, or 20 *in vitro* LNPs, how likely were we to pick the 1st, 1st and 2nd, or 1st, 2nd, and 3rd ranked *in vivo* LNPs? The odds of finding the top LNP for 3 *in vivo* endothelial cell beds were 11%, 22%, and 44% using the top 3, 5, and 20 *in vitro* LNPs, respectively; the odds of finding the top 2, or top 3 *in vivo* LNPs were lower (Fig. 4C). We performed the same analyses for *in vivo* macrophages from three tissues and obtained similar results (Fig. S4C). Taken together, these data strongly that *in vitro* delivery may not predict systemic *in vivo* delivery. While they do not directly implicate all *in vitro* systems or all cell types, they do strongly suggest each *in vitro* system should be validated using many nanoparticles before being used as the basis for nanoparticle discovery.

The JORDAN system generates large nanoparticle datasets; the size of these datasets enabled us to analyze the relationship between LNP properties and *in vivo* delivery. We plotted DNA barcode delivery as a function of each material property. In total, we analyzed 309 relationships between LNP structure and *in vivo* delivery. We found that the lipomer alkyl tail length, lipomer amine structure, and PEG molecular weight were most likely to influence LNP delivery (Fig. S4H). These results suggest that the structure of the amine-lipid compound, as well as the structure of PEG both strongly influence LNP targeting. These results provide an important insight into LNP library design and substantiate

previously reported nanoparticle research[35–37]. One important limitation is that we were not able to identify a mathematical framework with assumptions that allowed us to analyze how multiple LNP chemical variables interacted with one another. This future work is important, given that changing 1 LNP parameter often impacts another (e.g. adding more PEG to the LNP concomitantly reduces cholesterol).

Nanoparticle biodistribution is quantified using *ex vivo* tissue fluorescence; however, it is still unclear how different cell types within a tissue microenvironment are targeted[5, 16]. More specifically, it is unclear which cell types tend to be targeted by similar LNPs. To address this question, we focused on the spleen; LNPs can deliver nucleic acids to[38], and be cleared by[16], the spleen. We formulated a 4th LNP library. Library 4 consisted of 144 LNPs, of which 85 were found to be stable by DLS, and included (Fig. S5A, B). We administered library 4 to RAWs and mice, and isolated 8 different cell types using FACS (Fig. 5A, Fig. S5C). We performed unbiased Euclidean clustering, which is used to simultaneously compare how many experimental groups relate to one another (Fig. 5B). This technique is commonly used in bioinformatics to 'cluster' samples that share more similarity to one another than with other samples. Euclidean clustering recapitulated our results from libraries 1–3, separating *in vivo* delivery to all cell types (including macrophages) from *in vitro* delivery to RAWs (Fig. 5B, Fig. 5C, Fig. 5G).

Interestingly, the 7 immune cell sub-types clustered into cells derived from myeloid progenitors and lymphoid progenitors. Plasmacytoid and conventional dendritic cells were clustered most closely with one another, and also clustered closely with macrophages and neutrophils (Fig. 5B, Fig. 5C). All 4 cell types derive from a common progenitor. T cells, B cells, and natural killer cells, which derive from a different progenitor, clustered together (Fig. 5B, Fig. 5C). This suggests that nanoparticles which targeted 1 cell type derived from myeloid progenitors were more likely to target another cell type derived from myeloid progenitors, compared to a cell type derived from a lymphoid progenitor. To quantify this clustering, we measured the correlation between all tested cell types (Fig. 5C). Conventional DCs and plasmacytoid DCs, which clustered together, were highly correlated to each other ($R^2 = 0.90$) (Fig. 5C, 5D), as were B cells and T cells ($R^2 = 0.88$) (Fig. 5C, 5E). Cells derived from myeloid progenitors (e.g. conventional DCs) and lymphoid progenitors (e.g. T cells) had a much weaker correlation ($R^2 = 0.2$) (Fig 5F). These data demonstrate a unique capability for the JORDAN system; directly comparing how dozens of LNPs deliver nucleic to 7 different cell types would be very challenging using traditional one-by-one methods (e.g. fluorescence).

Using delivery data generated from this screen, we identified two LNPs for additional characterization (Fig. 6A). Barcodes delivered by LNP1 were enriched in all 8 splenic cell types, relative to barcodes delivered by LNP2 (Fig. 6B, C). We formulated LNP1 and LNP2 separately, using a Cy5.5-tagged DNA barcode, and injected mice intravenously with 0.75 mg/kg DNA barcode. LNP1-treated mice had 12.1x more splenic Cy5.5 *ex vivo* fluorescence than LNP2-treated mice, recapitulating the barcode readouts (Fig. 6D).

Discussion

We found that *in vivo* delivery to macrophages and endothelial cells is not predicted *in vitro* using common cell culture conditions. Modeling all the factors (e.g. blood flow, vascular heterogeneity, systemic and local immune cells, unwanted delivery to clearance organs) that influence nanoparticles *in vivo* is challenging. These results have important implications for nanoparticle design, given that nanoparticles are typically selected *in vitro*. We initially compared delivery to 5 different cell lines, and 6 different *in vivo* cell types; it will be important to determine whether these results extend to other cell types and cell culture conditions. For example, it was previously shown that delivery in primary hepatocytes was more predictive of *in vivo* delivery than a hepatoma cell line[39]. At first glance, our results may seem to contradict this work. We believe they do not; both studies underscore the importance of characterizing how well a given *in vitro* system predicts a desired *in vivo* outcome. To this end, we believe JORDAN is well positioned to optimize organ-on-a-chip[40] and organoids[41] designed to predict *in vivo* behavior by acting as a positive control.

JORDAN is agnostic to cell type and animal model. This allowed us to easily study drug delivery to 8 different splenic cell types in a single experiment. Testing how many LNPs target several cell types may lead to interesting discoveries. For example, our results suggest cells derived from myeloid progenitors tend to be targeted by the similar LNPs. This provides preliminary evidence that gene expression patterns that promote LNP delivery to phagocytic cells may be identified. However, these results need to be validated using other nanoparticles.

We noticed that there were practical advantages to using the JORDAN system. Testing many nanoparticles at once reduces experimental variation that occurs when experiments performed over months are compared to one another. We previously screened LNPs one by one[5]; it was difficult to ensure kits, reagents, and cell passage number were perfectly consistent. By testing many LNPs on the same day, it is easier to reduce unintentional experimental bias. At the same time, the JORDAN system has limitations. JORDAN is unlikely to work with unstable or toxic LNPs; it is critical to characterize particles before pooling them. JORDAN measures biodistribution, which is required, but not sufficient, for intracellular delivery. It will also be important to prevent PCR contamination. Finally, like all high throughput screening systems, lead candidates need to be independently verified. For example, we identified LNP1, which performed well in our barcode screen, and LNP2, which performed poorly in our barcode screen, before confirming their activity one by one (Figs. 5, 6). As part of our original barcoding study[18], we performed a similar confirmation experiment using Factor 7 siRNA.

Despite these caveats, our data demonstrate that JORDAN is a powerful new tool to help researchers understand *in vivo* drug delivery. We also believe the differences between *in vitro* and *in vivo* delivery suggest that *in vivo* screening may accelerate the rate at which clinically relevant LNPs can be discovered. To help other labs use the JORDAN system, we have published an open-source, ‘living’ document, which details reagents, protocols and our LNP bioinformatics pipeline on dahlmanlab.org.

Materials and Methods

Nanoparticle Formulation

Nanoparticles were formulated in a microfluidic device by mixing DNA with lipomer, PEG, cholesterol, and a helper lipid, as previously described[5, 18, 19, 22–27, 42]. Nanoparticles were made with variable mole ratios of these constituents. The genetic drug (in this case, DNA barcode) was diluted in 10 mM citrate buffer (Teknova), and loaded into a syringe (Hamilton Company). The materials making up the nanoparticle (lipomer, cholesterol, PEG, and helper lipid) were diluted in 100% ethanol, and loaded into a second syringe. The citrate phase and ethanol phase were mixed together in a microfluidic device, at rates of 600 uL/min and 200 uL/min, respectively, to form LNPs. We used the following helper lipids: DOPE (Avanti Lipids, 850725), and DOPC (Avanti Lipids, 850375).

DNA barcoding

Each chemically distinct LNP was formulated to carry its own unique DNA barcode (Fig. 1A, B). For example, LNP1 carried DNA barcode 1, while the chemically distinct LNP2 carried DNA barcode 2.

The DNA barcodes were designed rationally with several characteristics, as we previously described[18]. We purchased 56 nucleotide single stranded DNA sequences from IDT (Fig. 1C, Fig. S1A). We included 2 universal 21 and 20 nucleotide primer regions in addition to a random 7 nucleotide ('7N') region that is unique to each piece of DNA (Fig. S1B). Barcodes were distinguished using an 8 basepair (bp) sequence in the middle of the barcode. An 8 bp sequence can generate over 65,000 (4^8) unique barcodes; we selected 240 barcodes to prevent sequence bleaching on the Illumina MiniSeq™ machine. The 2 nucleotides on the 5′ and 3′ ends of the 56-nucleotide ssDNA sequence were modified with phosphorothioate linkages to reduce exonuclease degradation and improve DNA barcode stability.

Nanoparticle Characterization

LNP hydrodynamic diameter was measured using high throughput dynamic light scattering (DLS) (DynaPro Plate Reader II, Wyatt). LNPs were diluted in sterile 1X PBS to a concentration of ~0.0005 mg/mL, and analyzed. LNPs were included if they met 3 criteria: diameter >20 nm, diameter <300 nm, and autocorrelation function with only 1 inflection point. Over the course of our experiments, ~65% of the LNPs we formulated met all 3 criteria. Particles that met these criteria were pooled and dialyzed with 1X phosphate buffered saline (PBS, Invitrogen), and were sterile filtered with a 0.22 μm filter.

Animal Experiments

All animal experiments were performed in accordance with the Georgia Institute of Technology's Institutional Animal Care and Use Committee (IACUC). Female C57BL/6J (#000664) mice were purchased from the Jackson Laboratory. All mouse weights before and after injection, are shown in (Fig. S6A, B). In all experiments, mice were aged 4–12 weeks, female, and N = 3 – 5 mice per group were injected intravenously via the lateral tail vein with the same pooled LNPs.

Nanoparticle dosing

Mice were injected with a total DNA dose of 0.5 mg/kg. As an example, if an experiment measured 100 nanoparticles, then on average, each nanoparticle was administered at a dose of 0.005 mg/kg. The nanoparticle dose was determined using NanoDrop (Thermo Scientific).

Cell Culture

In vitro experiments were performed using mouse macrophage cells (RAW 264.7, ATCC), mouse aortic endothelial cells (provided by Hanjoong Jo at Emory)[34], primary human aortic endothelial cells (HAEC, Lonza), primary human umbilical vein endothelial cells (HUVEC, Lonza), and primary human aortic vein endothelial cells (HAVEC, Lonza).

In all cases, cells were maintained and cultured using previously established conditions. In all cases, cell media was supplemented by penicillin-streptomycin (500 U/mL penicillin G, 0.5 mg/mL streptomycin) (PenStrep, VWR) and 10% (v/v) fetal bovine serum (FBS, VWR). RAW cells were passaged with DMEM F-12 50/50 (Corning). iMAEC cells were passaged using DMEM with 1 g/L glucose, L-glutamine, and sodium pyruvate (Corning), supplemented by 1% (v/v) MEM non-essential amino acid solution (MEMNEAA, Sigma Aldrich), and 25 μg/mL endothelial cell growth supplement (ECGS, Emd Millipore). HAEC and HAVEC cells were passaged with MCDB 131 media without L-glutamine (VWR Scientific), supplemented by 1% (v/v) L-glutamate, 25 μg/mL ECGS, 0.1% (v/v) ascorbic acid, hydrocortisol, and the following growth factors: endothelial growth factor (EGF), vascular-endothelial growth factor (VEGF), fibroblast growth factor (FGF), and insulin-like growth factor (IGF). HUVEC cells were passaged with M199 media with Earle's salts and L-glutamine (Corning), supplemented by 1% (v/v) ECGS, L-glutamine, and 0.2% (v/v) heparin.

In all cases, cells were seeded in a 24 well plate at a density of 40,000 cells/well. 24 hours later, LNPs were added with a total DNA dose of 4, 20, or 100 ng (Fig. 2E, Fig. S2B–D). Based on these results, cells were treated with 20 ng total DNA in all other experiments. Six hours after transfection, media was removed, and fresh media was added. 72 hours after transfection, media was removed and DNA was isolated using QuickExtract (EpiCentre).

Fixed-cell staining

Cells were plated onto 35 mm glass-bottom dishes (In Vitro Scientific) one day prior to particle delivery. Cells were fixed at the indicated time points with 4% paraformaldehyde (Electron Microscopy Sciences) for 10 min at room temperature before permeabilization with 0.2% Triton X-100 (Sigma-Aldrich) for 5 min at room temperature. To stain actin, cells were then incubated with Phalloidin-488 (Thermo Scientific) for 30 minutes at 37°C. Nuclei were stained with 4′,6-diamidino-2-phenylindole (DAPI) (Life Technologies), and coverslips were placed over the cells in the dish and mounted with Prolong Gold (Life Technologies).

Microscopy

Images were acquired with a Hamamatsu Flash 4.0 v2 sCMOS camera on a PerkinElmer UltraView spinning disk confocal microscope mounted to a Zeiss Axiovert 200M body with a 63x NA 1.4 plan-apochromat objective. Images were acquired with Volocity (PerkinElmer) with Z-stacks taken in 0.2 μm increments. For live-cell images, cells and dishes were kept at 37 °C during imaging by using a Chamlide TC-L live-cell stage-top environment with objective heater (Live Cell Instrument). All images were linearly contrast enhanced. Live-cell images were smoothed with a fine rolling ball filter in Volocity.

Cell Isolation

One time-course experiment was performed; delivery was analyzed 4, 48, and 72 hours after LNPs were administered. In all other cases, tissues and cells were isolated 72 hours after injection with LNPs. In all experiments, mice were perfused with 20 mL of 1X PBS through the right atrium. The heart, lungs, spleen, and bone marrow were isolated immediately following perfusion. Tissues were finely cut, and then placed in a digestive enzyme solution with Collagenase Type I (Sigma Aldrich), Collagenase XI (Sigma Aldrich), and Hyaluronidase (Sigma Aldrich). The digestive enzyme for heart included Collagenase IV (Sigma Aldrich)[22]. Tissues were digested for 45 minutes at 37°C and 550 rpm. Digested tissues were passed through a 70 μm filter. Red blood cells were lysed using (RBC) lysis buffer. Cells were resuspended in FACS buffer (2% FBS in 1X PBS).

Heart, Lung, Bone Marrow Cell Staining

Cells were stained to identify specific cell populations and sorted using the BD FacsFusion and BD Facs Aria IIIu cell sorters in the Georgia Institute of Technology cellular analysis core. Antibodies used for staining were CD31 (clone 390, BioLegend), CD45.2 (clone 104, BioLegend), and CD11b (clone M1/70, BioLegend).

We defined cell populations in the following manner: macrophages ($CD31^{-}CD45^{+}CD11b^{+}$), heart and lung endothelial cells ($CD31^{+}CD45^{-}$), bone marrow endothelial cells ($CD31^{+}$) **(S3A–C).**

Splenic Cell Staining and Isolation

Splenocytes were isolated by digesting sliced spleens in 0.1 U/mL collagenase (Sigma Aldrich) in Hank's Balanced Salt Solution (Corning) for 30 minutes at 37°C. Digestion was stopped by addition of EDTA to 5 mM, and the resulting mixture was passed through a cell strainer. Red blood cells were removed with ACK lysing buffer (Lonza), and cells were washed in FACS buffer (PBS supplemented with 2% FBS and 2 mM EDTA; Corning and HyClone) and re-strained.

Cells were stained by conventional methods in FACS buffer as previously described[43]. Antibodies used for staining were CD19 (clone 1D3, eBioscience), CD3 (clone 17A2, eBioscience), CD31 (clone 390, BioLegend), CD45 (clone 104, BioLegend), NK1.1 (clone PK136, eBioscience), CD11b (clone M1/70, BioLegend), CD11c (clone N418, BioLegend), Siglec H (clone 551, BioLegend), F4/80 (clone BM8, BioLegend), and Ly-6G (clone 1A8,

BioLegend). Cells were also stained with LIVE/DEAD viability dyes (Thermo Fisher) to exclude dead cells.

Described splenocyte cell types (Fig. 5A, Fig. S5C) from four mice were isolated by FACS on two FACSAria II cell sorters (BD Biosciences) at the Emory University School of Medicine Flow Cytometry Core.

PCR Amplification

All samples were amplified and prepared for sequencing. More specifically, 1μL of primers (5uM for Final Reverse/Forward, 0.5uM for Base Forward) were added to 5 μL of Kapa HiFi 2X master mix, 3 μL sterile H_2O, and 1 μL DNA template. The reaction was run for 30 cycles. When the PCR reaction did not produce clear bands, the primer concentrations, DNA template input, PCR temperature, and number of cycles were optimized for individual samples. The PCR amplicon was isolated with gel extraction.

Deep Sequencing

Illumina deep sequencing was conducted in Georgia Tech's Molecular Evolution core. Runs were performed on an Illumina Miniseq™. Primers were designed based on Nextera XT adapter sequences.

Data Normalization

Counts for each particle, per tissue, were normalized to unity (Fig. 1D) The DNA counts in each tissue were then normalized to 100%. For example, if a sample (e.g. heart1) had 500,000 total barcode reads, and 50,000 of them came from particle X, while 4,000 came from particle Y, then the normalized delivery for particle X and Y would be 10% and 0.8%, respectively. The barcoded LNP mixture we injected into the mouse was also sequenced. This 'input' DNA was used to normalize DNA counts from the cells and tissues (Fig. S1C).

Data Analysis

Sequencing results were processed using a custom python-based tool to extract raw barcode counts for each tissue. These raw counts were then normalized with an R script prior to further analysis. Statistical analysis was done using GraphPad Prism 7. Correlation analyses were run assuming a Gaussian distribution in order to obtain Pearson correlation coefficients. R^2 values (0 – 1) were computed by squaring Pearson correlation coefficients.

Data Access

The data, analyses, and scripts used to generate all figures in the paper are available upon request to J.E.D. or dahlmanlab.org.

Supplementary Material

Refer to Web version on PubMed Central for supplementary material.

Acknowledgments

The authors thank Jordan Cattie, Gabriel Kwong, Melissa Kemp, Marwa Mahmoud, Hanjoong Jo, and Timothy Mark O'Shea for providing helpful feedback, as well as cells and reagents. The authors thank Sommer Durham and the Georgia Tech Cellular Analysis and Cytometry Core. The authors thank Robert Karaffa, Conner Carter, and the Emory University School of Medicine Flow Cytometry Core. Finally, J.E.D. thanks Taylor E. Shaw.

Funding. C.D.S., K.P., and J.E.D. were funded by Georgia Tech startup funds (awarded to J.E.D.) C.M.M. was funded by the Georgia Research Assistantship (Grant 3201330). K.P. was also funded by the NIH/NIGMS-sponsored Cell and Tissue Engineering (CTEng) Biotechnology Training Program (T32GM008433). C.D.S. was also funded by the NIH/NIGMS-sponsored Immunoengineering Training Program (T32EB021962). W.H.H is a Cancer Research Institute Irvington Fellow supported by the Cancer Research Institute. Research was funded by the Cystic Fibrosis Research Foundation (DAHLMA15XX0, awarded to J.E.D.), the Parkinson's Disease Foundation (PDF-JFA-1860, awarded to J.E.D.), and the Bayer Hemophilia Awards Program (AGE DTD, awarded to J.E.D.). This study was also supported with funding from the National Institutes of Health GT BioMAT Training Grant under Award Number (5T32EB006343). This work was performed in part at the Georgia Tech Institute for Electronics and Nanotechnology, a member of the National Nanotechnology Coordinated Infrastructure, which is supported by the National Science Foundation (Grant ECCS-1542174).

References

1Blanco E, Shen H, Ferrari M. Nat Biotechnol. 2015; 33(9):941–51. [PubMed: 26348965]

2Cheng CJ, Tietjen GT, Saucier-Sawyer JK, Saltzman WM. Nat Rev Drug Discov. 2015; 14(4):239–47. [PubMed: 25598505]

3Sahin U, Kariko K, Tureci O. Nat Rev Drug Discov. 2014; 13(10):759–80. [PubMed: 25233993]

4Dong Y, Love KT, Dorkin JR, Sirirungruang S, Zhang Y, Chen D, Bogorad RL, Yin H, Chen Y, Vegas AJ, Alabi CA, Sahay G, Olejnik KT, Wang W, Schroeder A, Lytton-Jean AK, Siegwart DJ, Akinc A, Barnes C, Barros SA, Carioto M, Fitzgerald K, Hettinger J, Kumar V, Novobrantseva TI, Qin J, Querbes W, Koteliansky V, Langer R, Anderson DG. Proceedings of the National Academy of Sciences of the United States of America. 2014; 111(11):3955–60. [PubMed: 24516150]

5Dahlman JE, Barnes C, Khan OF, Thiriot A, Jhunjunwala S, Shaw TE, Xing Y, Sager HB, Sahay G, Speciner L, Bader A, Bogorad RL, Yin H, Racie T, Dong Y, Jiang S, Seedorf D, Dave A, Singh Sandhu K, Webber MJ, Novobrantseva T, Ruda VM, Lytton-JeanAbigail KR, Levins CG, Kalish B, Mudge DK, Perez M, Abezgauz L, Dutta P, Smith L, Charisse K, Kieran MW, Fitzgerald K, Nahrendorf M, Danino D, Tuder RM, von Andrian UH, Akinc A, Panigrahy D, Schroeder A, Koteliansky V, Langer R, Anderson DG. Nat Nano. 2014; 9(8):648–655.

6Love KT, Mahon KP, Levins CG, Whitehead KA, Querbes W, Dorkin JR, Qin J, Cantley W, Qin LL, Racie T, Frank-Kamenetsky M, Yip KN, Alvarez R, Sah DW, de Fougerolles A, Fitzgerald K, Koteliansky V, Akinc A, Langer R, Anderson DG. Proceedings of the National Academy of Sciences of the United States of America. 2010; 107(5):1864–9. [PubMed: 20080679]

7Akinc A, Zumbuehl A, Goldberg M, Leshchiner ES, Busini V, Hossain N, Bacallado SA, Nguyen DN, Fuller J, Alvarez R, Borodovsky A, Borland T, Constien R, de Fougerolles A, Dorkin JR, Narayanannair Jayaprakash K, Jayaraman M, John M, Koteliansky V, Manoharan M, Nechev L, Qin J, Racie T, Raitcheva D, Rajeev KG, Sah DW, Soutschek J, Toudjarska I, Vornlocher HP, Zimmermann TS, Langer R, Anderson DG. Nat Biotechnol. 2008; 26(5):561–9. [PubMed: 18438401]

8Hao J, Kos P, Zhou K, Miller JB, Xue L, Yan Y, Xiong H, Elkassih S, Siegwart DJ. J Am Chem Soc. 2015; 29:9206–9209. 1520–5126 (Electronic).

9Siegwart DJ, Whitehead KA, Nuhn L, Sahay G, Cheng H, Jiang S, Ma M, Lytton-Jean A, Vegas A, Fenton P, Levins CG, Love KT, Lee H, Cortez C, Collins SP, Li YF, Jang J, Querbes W, Zurenko C, Novobrantseva T, Langer R, Anderson DG. Proceedings of the National Academy of Sciences of the United States of America. 2011; 108(32):12996–3001. [PubMed: 21784981]

10Zuckerman JE, Choi CH, Han H, Davis ME. Proc Natl Acad Sci U S A. 2012; 109(8):3137–42. [PubMed: 22315430]

11Aird WC. Critical care medicine. 2003; 31(4):S221–S230. [PubMed: 12682444]

12Aird WC. Cold Spring Harbor perspectives in medicine. 2012; 2(1):a006429. [PubMed: 22315715]

13Aird WC. Circulation research. 2007; 100(2):174–190. [PubMed: 17272819]

14Aird WC. Circulation research. 2007; 100(2):174–190. [PubMed: 17272819]

15Augustin HG, Koh GY. Science. 2017; 357(6353):eaal2379. [PubMed: 28775214]

16Tsoi KM, MacParland SA, Ma XZ, Spetzler VN, Echeverri J, Ouyang B, Fadel SM, Sykes EA, Goldaracena N, Kaths JM, Conneely JB, Alman BA, Selzner M, Ostrowski MA, Adeyi OA, Zilman A, McGilvray ID, Chan WC. Nat Mater. 2016; 15(11):1212–1221. [PubMed: 27525571]

17Zhang Y, Sloan SA, Clarke LE, Caneda C, Plaza CA, Blumenthal PD, Vogel H, Steinberg GK, Edwards MS, Li G, Duncan JA 3rd, Cheshier SH, Shuer LM, Chang EF, Grant GA, Gephart MG, Barres BA. Neuron. 2016; 89(1):37–53. [PubMed: 26687838]

18Dahlman JE, Kauffman KJ, Xing Y, Shaw TE, Mir FF, Dlott CC, Langer R, Anderson DG, Wang ET. Proceedings of the National Academy of Sciences of the United States of America. 2017; 114(8):2060–2065. [PubMed: 28167778]

19Chen D, Love KT, Chen Y, Eltoukhy AA, Kastrup C, Sahay G, Jeon A, Dong Y, Whitehead KA, Anderson DG. J Am Chem Soc. 2012; 134(16):6948–51. [PubMed: 22475086]

20Carmeliet P, Jain RK. Nature. 2011; 473(7347):298–307. [PubMed: 21593862]

21Swirski FK, Nahrendorf M. Science. 2013; 339(6116):161–6. [PubMed: 23307733]

22Sager HB, Dutta P, Dahlman JE, Hulsmans M, Courties G, Sun Y, Heidt T, Vinegoni C, Borodovsky A, Fitzgerald K, Wojtkiewicz GR, Iwamoto Y, Tricot B, Khan OF, Kauffman KJ, Xing Y, Shaw TE, Libby P, Langer R, Weissleder R, Swirski FK, Anderson DG, Nahrendorf M. Science translational medicine. 2016; 8(342):342ra80–342ra80.

23Yun S, Budatha M, Dahlman JE, Coon BG, Cameron RT, Langer R, Anderson DG, Baillie G, Schwartz MA. Nat Cell Biol. 2016

24Xue W, Dahlman JE, Tammela T, Khan OF, Sood S, Dave A, Cai W, Chirino LM, Yang GR, Bronson R, Crowley DG, Sahay G, Schroeder A, Langer R, Anderson DG, Jacks T. Proceedings of the National Academy of Sciences. 2014; 111(34):E3553–E3561.

25Platt RJ, Chen S, Zhou Y, Yim MJ, Swiech L, Kempton HR, Dahlman JE, Parnas O, Eisenhaure TM, Jovanovic M, Graham DB, Jhunjhunwala S, Heidenreich M, Xavier RJ, Langer R, Anderson DG, Hacohen N, Regev A, Feng G, Sharp PA, Zhang F. Cell. 2014; 159(2):440–55. [PubMed: 25263330]

26Sager HB, Hulsmans M, Lavine KJ, Moreira MB, Heidt T, Courties G, Sun Y, Iwamoto Y, Tricot B, Khan OF, Dahlman JE, Borodovsky A, Fitzgerald K, Anderson DG, Weissleder R, Libby P, Swirski FK, Nahrendorf M. Circ Res. 2016; 119(7):853–64. [PubMed: 27444755]

27White K, Lu Y, Annis S, Hale AE, Chau BN, Dahlman JE, Hemann C, Opotowsky AR, Vargas SO, Rosas I, Perrella MA, Osorio JC, Haley KJ, Graham BB, Kumar R, Saggar R, Saggar R, Wallace WD, Ross DJ, Khan OF, Bader A, Gochuico BR, Matar M, Polach K, Johannessen NM, Prosser HM, Anderson DG, Langer R, Zweier JL, Bindoff LA, Systrom D, Waxman AB, Jin RC, Chan SY. EMBO Mol Med. 2015; 7(6):695–713. [PubMed: 25825391]

28Khan OF, Zaia EW, Jhunjhunwala S, Xue W, Cai W, Yun DS, Barnes CM, Dahlman JE, Dong Y, Pelet JM, Webber MJ, Tsosie JK, Jacks TE, Langer R, Anderson DG. Nano Lett. 2015; 15(5): 3008–16. [PubMed: 25789998]

29Khan OF, Zaia EW, Yin H, Bogorad RL, Pelet JM, Webber MJ, Zhuang I, Dahlman JE, Langer R, Anderson DG. Angew Chem Int Ed Engl. 2014; 53(52):14397–401. [PubMed: 25354018]

30Wittrup A, Ai A, Liu X, Hamar P, Trifonova R, Charisse K, Manoharan M, Kirchhausen T, Lieberman J. Nat Biotechnol. 2015

31Gilleron J, Querbes W, Zeigerer A, Borodovsky A, Marsico G, Schubert U, Manygoats K, Seifert S, Andree C, Stoter M, Epstein-Barash H, Zhang L, Koteliansky V, Fitzgerald K, Fava E, Bickle M, Kalaidzidis Y, Akinc A, Maier M, Zerial M. Nat Biotechnol. 2013; 31(7):638–46. [PubMed: 23792630]

32Geary RS, Norris D, Yu R, Bennett CF. Adv Drug Deliv Rev. 2015; 87:46–51. [PubMed: 25666165]

33Crooke ST, Wang S, Vickers TA, Shen W, Liang XH. Nat Biotechnol. 2017; 35(3):230–237. [PubMed: 28244996]

34Ni CW, Kumar S, Ankeny CJ, Jo H. Vascular cell. 2014; 6(1):7. [PubMed: 24690145]

35Kumar V, Qin J, Jiang Y, Duncan RG, Brigham B, Fishman S, Nair JK, Akinc A, Barros SA, Kasperkovitz PV. Mol Ther Nucleic Acids. 2014; 3:e210. [PubMed: 25405467]

36Tao W, Davide JP, Cai M, Zhang GJ, South VJ, Matter A, Ng B, Zhang Y, Sepp-Lorenzino L. Mol Ther. 2010; 18(9):1657–66. [PubMed: 20628357]

37Mui BL, Tam YK, Jayaraman M, Ansell SM, Du X, Tam YY, Lin PJ, Chen S, Narayanannair JK, Rajeev KG, Manoharan M, Akinc A, Maier MA, Cullis P, Madden TD, Hope MJ. Mol Ther Nucleic Acids. 2013; 2:e139. [PubMed: 24345865]

38Kranz LM, Diken M, Haas H, Kreiter S, Loquai C, Reuter KC, Meng M, Fritz D, Vascotto F, Hefesha H, Grunwitz C, Vormehr M, Husemann Y, Selmi A, Kuhn AN, Buck J, Derhovanessian E, Rae R, Attig S, Diekmann J, Jabulowsky RA, Heesch S, Hassel J, Langguth P, Grabbe S, Huber C, Tureci O, Sahin U. Nature. 2016; 534(7607):396–401. [PubMed: 27281205]

39Whitehead KA, Matthews J, Chang PH, Niroui F, Dorkin JR, Severgnini M, Anderson DG. ACS nano. 2012; 6(8):6922–9. [PubMed: 22770391]

40Bhatia SN, Ingber DE. Nat Biotechnol. 2014; 32(8):760–72. [PubMed: 25093883]

41Fatehullah A, Tan SH, Barker N. Nat Cell Biol. 2016; 18(3):246–254. [PubMed: 26911908]

42Koga J, Nakano T, Dahlman JE, Figueiredo JL, Zhang H, Decano J, Khan OF, Niida T, Iwata H, Aster JC, Yagita H, Anderson DG, Ozaki CK, Aikawa M. Arteriosclerosis, thrombosis, and vascular biology. 2015; 35(11):2343–53.

43Araki K, Morita M, Bederman AG, Konieczny BT, Kissick HT, Sonenberg N, Ahmed R. Nature immunology. 2017; 18(9):1046–1057. [PubMed: 28714979]

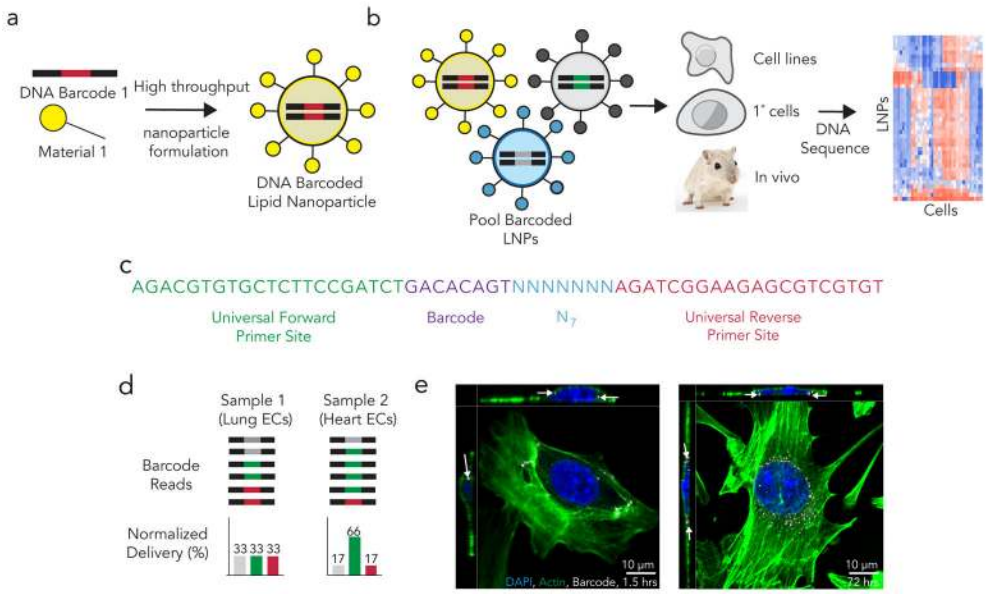

Figure 1.

JOint Rapid Dna Analysis of Nanoparticles (JORDAN), a system for high throughput *in vivo* nanoparticle analysis. **(a)** Lipid nanoparticles (LNPs) were formulated to carry DNA barcodes, before **(b)** stable LNPs were pooled together and administered to cells or mice. Cells were deep sequenced to quantify the relative delivery of all the LNPs simultaneously. **(c)** The DNA barcode was rationally designed with universal primer sites and a randomized 7 nucleotide region to minimize PCR bias. **(d)** Normalized delivery for every barcoded LNP was calculated. In this example schematic, all 3 barcodes were equally represented in Sample 1, while in Sample 2, the green barcode was overrepresented. We would hypothesize that the gray LNP delivered DNA more efficiently to Sample 2 than the yellow or blue LNP. The full data analysis to calculate normalized delivery is described in Supplementary Fig. 1C. **(e)** Alexa-647 fluorescence 1.5 and 72 hours after cells were transfected with 20 ng of Alexa Fluor 647 tagged DNA barcode formulated into the LNP 7C1.

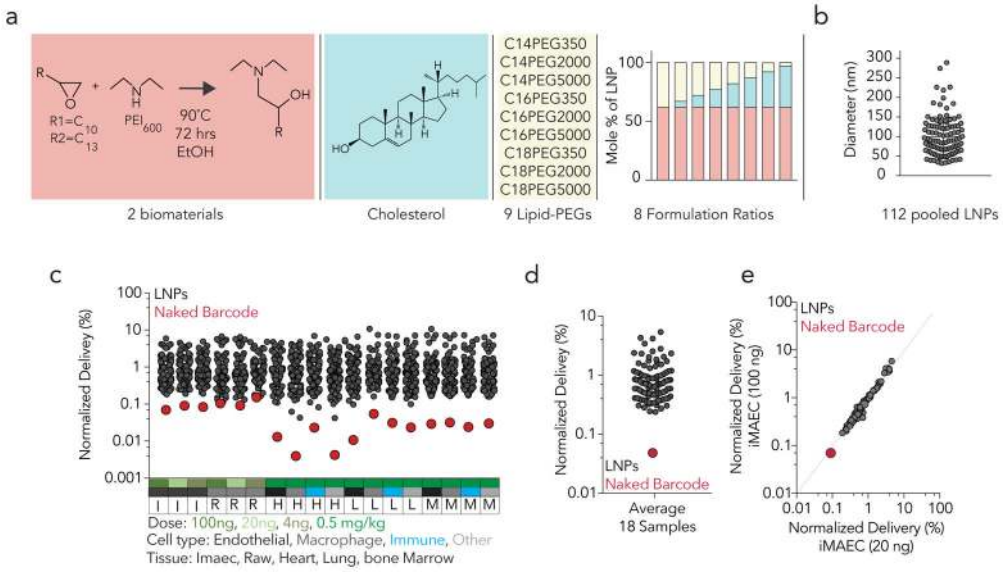

Figure 2.

To analyze the robustness of our system **(a)** We formulated 144 chemically distinct LNPs, **(b)** pooled stable LNPs and administered them to two cell lines (RAWs, iMAECs) and mice. **(c)** Normalized delivery for all LNPs and naked barcode in 18 cell and tissue types. **(d)** Average normalized delivery for all 18 samples. The naked barcode delivered DNA less efficiently than all LNPs. **(e)** Normalized delivery in iMAECs 72 hours after 20 ng or 100 ng total DNA was administered. *In vitro* delivery to iMAECs at 20 ng/well predicted *in vitro* delivery to iMAECs at 100 ng/well.

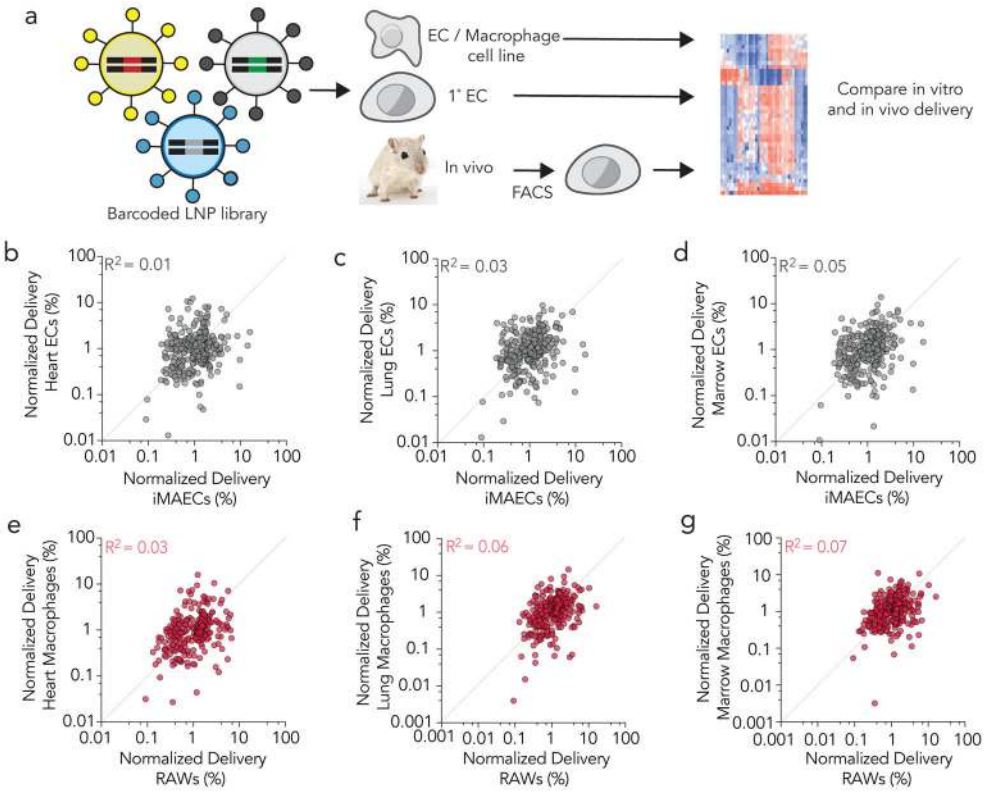

Figure 3.

A direct comparison between in vitro and in vivo nanoparticle delivery. **(a)** 420 LNPs were formulated and delivery was compared between in vivo FACS sorted cells, primary cells, and cell lines. **(b–d)** Normalized delivery of LNPs in iMAECs and heart, lung, and bone marrow endothelial cells. **(e–g)** Normalized delivery of LNPs in RAWs and heart, lung, and bone marrow macrophages. In both cases, in vitro LNP delivery does not predict in vivo delivery.

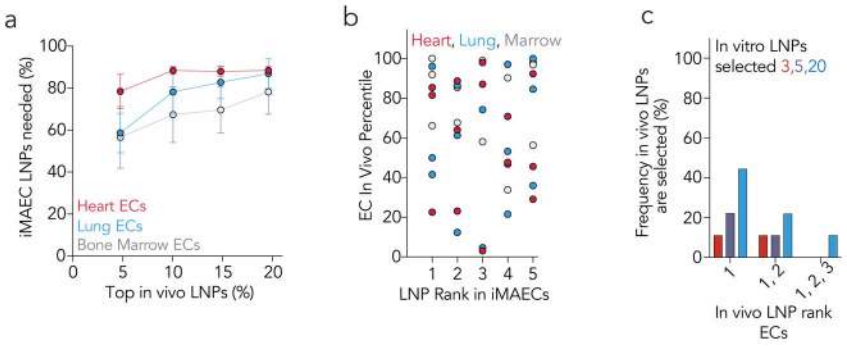

Figure 4.

Quantifying the efficiency with which *in vitro* screens predict *in vivo* delivery. **(a)** Percentage of *in vitro* LNPs required to encompass the top 5, 10, 15, and 20% of the LNPs in heart, lung, and bone marrow endothelial cells *in vivo*. For example, over 50% of the *in vitro* library would be required to ensure the top 5% of the *in vivo* LNPs were selected. **(b)** LNP rank *in vivo* in heart, lung, and bone marrow endothelial cells, for the top 5 *in vitro* ranked LNPs. **(c)** Frequency with which the 1st, 1st and 2nd, or 1st, 2nd, and 3rd *in vivo* LNPs would be chosen by selecting the top 3, 5, and 20 LNPs *in vitro*.

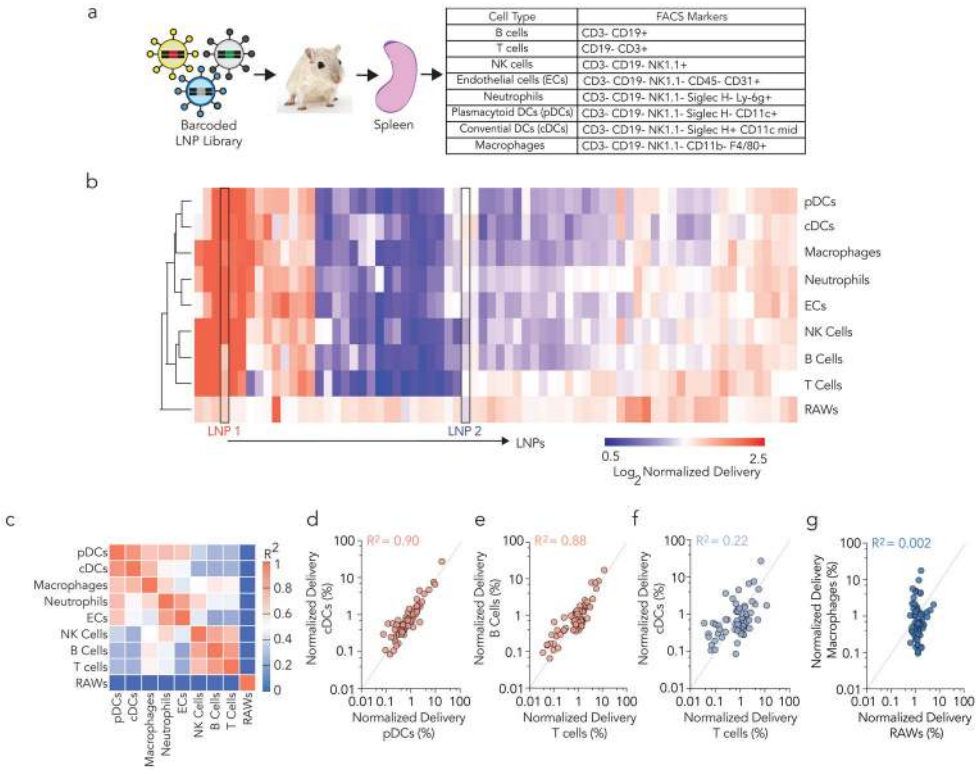

Figure 5.

High throughput analysis of delivery to splenic microenvironment. **(a)** 144 LNPs were formulated; 85 stable LNPs were pooled and administered to WT mice. 72 hours later, cell types were isolated from the spleen using FACS. **(b)** Unbiased clustering of LNPs in each cell type, generated by a Euclidean distance algorithm. RAWs (macrophage *in vitro*) clustered separately from all 8 *in vivo* cell types, and both dendritic cell populations clustered together. **(c)** R^2 values for all 8 *in vivo* cell types as well as RAWs. Normalized delivery in **(d)** plasmacytoid and conventional dendritic cells (DCs), **(e)** B cells and T cells, **(f)** conventional DCs and T cells, and **(g)** RAWs and splenic macrophages.

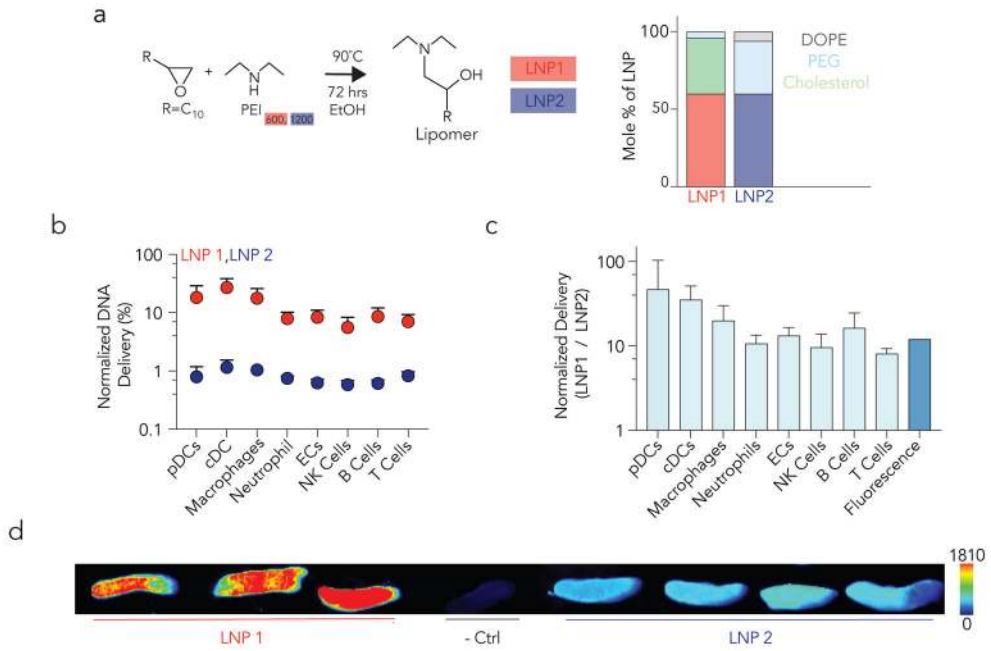

Figure 6.

(a) Chemical compositions of LNP1 and LNP2. **(b)** Normalized delivery of 2 LNPs; 1 with high (LNP1) and 1 with low (LNP2) normalized delivery. **(c)** The ratio of normalized delivery (LNP1/LNP2) in each cell type using barcodes, as well as fluorescence of the spleen whole tissue. **(d)** Cy5.5 fluorescence in splenic whole tissue 3 hours after mice were injected with either LNP1 or LNP2. LNP1 fluorescence was higher, as predicted by the barcoding data.